Appl. Phys. A (2015) 119:1413–1422
DOI 10.1007/s00339-015-9114-3

Applied Physics A
Materials Science & Processing

Study of synergistic effect among photo-, electro-, and sonoprocesses in photocatalyst degradation of phenol on tungsten-loaded titania nanotubes composite electrode

Mohamad Mohsen Momeni[1]

Received: 27 November 2014 / Accepted: 17 March 2015 / Published online: 27 March 2015

Abstract The degradation of 4-nitrophenol (4-NP) in aqueous solution with different processes was investigated. Tungsten-loaded titania nanotubes (WT-NTs) were used as electrode in photocatalytic (PC), sonophotocatalytic (SPC), photoelectrocatalytic (PEC), and sonophotoelectrocatalytic (SPEC) processes. WT-NTs electrode was fabricated by in situ anodization of titanium in a single-step process using sodium tungstate as the tungsten source. The morphology and structure were characterized by FE-SEM, XRD, and EDX. Experimental results showed that the hybrid processes could efficiently enhance the degradation efficiency of 4-NP and followed pseudo-first-order kinetics. At the optimized experimental conditions, the rate constants of degradation of 4-NP were 0.0594 min^{-1} for SPEC process, 0.0293 min^{-1} for PEC process, 0.0211 min^{-1} for SPC process, and 0.0116 min^{-1} for PC process. The rate constants indicated that there existed synergistic effect in the ultrasonic, electro-assisted, and photocatalytic processes.

1 Introduction

Heterogeneous photocatalysis using semiconductor oxides, an "advanced oxidative process (AOP)," is a very effective method for degradation of refractory organic pollutants to harmless compounds and can be considered a promising alternative for the final stage in wastewater treatment. The photocatalysis, with TiO_2 as the semiconductor photocatalyst, has emerged as a promising technique due to unique properties of TiO_2. Among the various treatment methods, AOP hybrid techniques such as photocatalytic ozonation, sonophotocatalytic (SPC), photoelectrocatalytic (PEC), photo-Fenton, electro-Fenton are promising for elimination and enhanced mineralization of pollutants [1, 2]. Although photocatalytic (PC) process using semiconductor as photocatalyst under light illumination has been extensively studied, its practical exploitation for the oxidation of organic pollutant has been restricted due to the low photonic efficiency [2, 3]. The fast recombination of the photogenerated electron/hole represents the major drawback of photocatalytic process applications. Therefore, it is important to retard the recombination of the charge carriers [2–4].

Photoelectrocatalytic (PEC) technology that is combination of electrochemical and photocatalysis technologies offers the opportunity to separate electron–hole photogenerated and to prevent their recombination. The semiconductors such as TiO_2 have conduction band and valence band. Upon radiation photons with energy greater than the band gap, the electrons are excited from the valence band to the conduction band, generating the electron–hole pairs [5, 6]:

$$TiO_2 + h\upsilon \rightarrow e^- + h^+. \quad (1)$$

The above reaction produces powerful oxidant (h^+), reacts with other oxidizable species (such as 4-nitrophenol), and degrades them. One of the main products comes from the oxidation of water molecules or hydroxyl ions and produces very active hydroxyl radicals

$$h^+ + H_2O \rightarrow {}^{\cdot}OH + H^+ \quad (2)$$

$$h^+ + OH^- \rightarrow {}^{\cdot}OH. \quad (3)$$

The hydroxide radical ($^{\cdot}OH$) is an active oxidant which reacts with substrates (S):

✉ Mohamad Mohsen Momeni
mm.momeni@cc.iut.ac.ir

[1] Department of Chemistry, Isfahan University of Technology, 84156-83111 Isfahan, Iran

$$S + {}^{\cdot}\mathrm{OH} \rightarrow \text{oxidation products.} \quad (4)$$

The major limit of photocatalysis efficiency comes from recombination of electron–hole pairs or reaction between the photogenerated electrons and the hydroxyl radicals through the following pathways:

$$h^{+} + e^{-} \rightarrow \text{heat} \quad (5)$$

$$e^{-} + {}^{\cdot}\mathrm{OH} \rightarrow \mathrm{OH}^{-}. \quad (6)$$

The applied bias potential to the working electrode prevents these two reactions by driving the photogenerated electrons to the auxiliary electrode (Pt), which resulted in better separation of the electron–hole pairs and thus decreases the electron–hole recombination [5, 6].

Sonochemistry generally involves the chemical effects of ultrasound that arise when a sound wave is passed through an aqueous medium. Often, the generation of highly reactive radical species such as ${}^{\cdot}H$ and ${}^{\cdot}\mathrm{OH}$ is observed as a consequence of the homolytic cleavage of water within the cavitation bubbles. Once these active radicals are formed, they non-selectively attack any organic pollutant present in the water phase and convert them into a variety of products [7]. In the presence of ultrasonic waves, organic compounds in water are degraded via several mechanisms. Three main pathways, which involve hydroxyl radical oxidation, pyrolytic degradation, and supercritical water reactions, have been proposed [7]. In recent years, there has been a remarkable interest in application of ultrasound to the degradation of organic pollutants. Sonolysis can convert ideally the organic pollutants to carbon dioxide and water or convert them to compounds which are less harmful than the original pollutants. Ultrasound can be used alone or in conjunction with other techniques. Sonochemical degradation takes a long processing time in order to achieve complete mineralization. Therefore, a sonolytic process combined with other techniques can be a promising way for the degradation/mineralization of pollutants.

Sonophotocatalytic (SPC) reaction is a photocatalytic reaction with ultrasonic irradiation or the simultaneous irradiation of ultrasound and light with a photocatalyst. The combination of ultrasound with a photocatalyst (such as TiO_2) degrades the target pollutant by an additional generation of hydroxyl radicals through both excitation of TiO_2 (reactions 1–3) and sonolytic splitting of water molecules (reactions 7–9). The important advantage of this combination process is that ultrasound continuously cleans the photocatalyst and is useful in maintaining its reactivity over longer irradiation times [7].

$$\mathrm{H_2O} \xrightarrow{\text{ultrasound}} {}^{\cdot}H + {}^{\cdot}\mathrm{OH} \quad (7)$$

$${}^{\cdot}\mathrm{OH} + {}^{\cdot}\mathrm{OH} \rightarrow \mathrm{H_2O_2} \quad (8)$$

$$\mathrm{H_2O_2} + {}^{\cdot}H \rightarrow \mathrm{H_2O} + {}^{\cdot}\mathrm{OH} \quad (9)$$

The sonophotoelectrocatalytic (SPEC) technology is combination of electrochemical, photocatalytic, and sonolytic technologies, and it is expected that in comparison with the double hybrid method, it be more efficient. Zhang et al. [8] showed that by means of simultaneous ultrasound and ultraviolet irradiation with electro-assisted way in the presence of TiO_2 electrode, photocatalytic degradation efficiency of methyl orange in aqueous solutions significantly increased.

Degradation of phenols is a matter of great interest since these compounds, which are found in the wastewater from several industries, are carcinogenic to mammals [9–13]. Phenols decomposition and mineralization in wastewater are possible by the application of new technologies such as adsorption, ozone oxidation, electrochemical degradation, and photocatalytic oxidation [14]. Photocatalysis is considered as a promising approach for the removal of 4-NP [15–17]. In 2006, Kidak et al. [18] reviewed the applications of ultrasound for the destruction of phenol and substituted phenols. However, many reports reflect that a common drawback of the sonochemical process is that the degradation degrees of phenol and substituted phenols are very low. To overcome this limitation, hybrid techniques utilizing sonication and a secondary process such as sonication/H_2O_2, sonication/Fenton, sonication/microwave, Hydrodynamic–Acoustic–Cavitation, sonication/H_2O_2/O_3 with zero valent metals and the combination of ultrasound and electrochemistry process have been used [19–24].

In recent years, TiO2 nanotube arrays have drawn increasing attention because they not only possess high surface areas but also offer the advantage of directed carrier transport facilitating the collection of photogenerated charge carriers and therefore are expected to be promising high-performance materials for use in photocatalysis. However, the application of TiO_2 nanotubes is limited by its high band gap energy (3.2 eV), which diminishes its absorption in the visible light range of solar spectrum. Also, the high photoinduced charge recombination rate and low charge separation is one main drawback that limits the photocatalytic efficiency of TiO_2 nanotubes. To overcome this problem, doping TiO_2 nanotubes with various metal or non-metal elements has been carried out [25–36]. A great deal of research has been directed toward using tungsten to modify different form of TiO_2 because the tungsten ion is considered one of best elements for narrowing the band gap of TiO_2 [22, 23]. Because W^{6+} has an ionic radius similar to that of Ti^{4+}, WO_3 can couple into TiO_2 crystals in their co-crystallization process during annealing, resulting in a well-doped WO_3–TiO_2 composite. Tungsten has a high charge state with six electrons in the outer orbit, and its ionic radius was 0.60 Å and was similar to that of Ti^{4+} (0.605 Å); thus, tungsten atom could substitute easily the

titanium atom in TiO_2 lattice [35]. Lewera et al. [37] fixed TiO_2 with WO_3, but the catalyst was easily lost during photocatalysis. Lai et al. [38] utilized the plasma electrolytic method to fabricate tungsten-loaded TiO_2 nanotubes; however, special equipment was required to achieve the spluttering coating. Das et al. [39] achieved tungsten-doped TiO_2 nanotubes using alloys but encountered difficulty in adjusting the dopant concentration. Therefore, a simple, facile, and inexpensive method of synthesizing tungsten-doped TiO_2 nanotubes is necessary.

In the present study, tungsten-loaded titania nanotubes (WT-NTs) were fabricated by a single-step anodization of titanium substrate in an organic bath consisted of DMSO/fluoride electrolyte containing sodium tungstate. Then, this electrode was used not only as photocatalyst in photocatalytic and sonophotocatalytic processes but also as photoelectrode in photoelectrocatalytic and sonophotoelectrocatalytic processes. The photocatalytic activities of WT-NTs were evaluated by degradation of 4-nitrophenol (4-NP). To our knowledge, the degradation of 4-NP by photocatalysis with WT-NTs has not been reported. The morphology and structure of WT-NTs were characterized by scanning electron microscopy (SEM), energy-dispersive X-ray spectroscopy (EDS), and X-ray diffraction (XRD). Optical properties were investigated by UV–Vis diffuse reflectance spectra (UV/vis/DRS).

2 Experimental

WT-NTs were synthesized by anodic oxidation of titanium in a mixture electrolyte, which was mixing DMSO and HF (98 mL DMSO + 1 mL HF +1 mL H_2O), followed by the dissolution 0.12 mM of sodium tungstate. The anodization experiments were carried out using a conventional two-electrode system with titanium foil as anode and platinum foil as cathode. Anodization was carried out under a constant voltage of 40 V for 8 h at room temperature. After anodization, the as-formed samples were annealed in oxygen atmosphere at 400 °C for 2 h (1 °C/min) to obtain crystalline WT-NTs.

The surface morphology of this sample was characterized by field emission scanning electron microscopy (FE-SEM, Hitachi S-4160, Japan), and the elemental composition was estimated by energy-dispersive X-ray spectroscopy (EDX). The crystalline phases were identified by XRD (Philips ẌPert). UV–visible absorption spectra of the samples were recorded on a photospectrometer (JASCO V-570).

Photocatalytic activities of samples were evaluated by degradation of the aqueous 4-nitrophenol (4-NP) under visible light irradiation. The photocatalytic reaction was carried in a single-compartment cylindrical quartz reactor. The photoreactor was immersed in the KQ ultrasonic cleaning bath model 3200DA (Kunshan ultrasonic instrument Corp. China). A 200-W Xenon lamp was used as a light source with a 420-nm cutoff filter to provide visible light. The luminous intensity of this lamp was 100 mW/cm^2. The initial concentration of 4-NP was 2 mg/L. The volume of the solution was 50 mL. Prior to illumination, the photocatalyst nanotube sample was immersed in quartz reactor containing 4-NP and magnetically stirred for 2 h in the dark to ensure the establishment of an adsorption–desorption equilibrium between the photocatalyst and 4-NP. Then, the solution was exposed to visible light irradiation. At specified intervals, 5 ml solution was sampled and the absorbance of 4-NP was measured by a UV–Vis spectrophotometer.

3 Results and discussion

3.1 Characterization of WT-NTs photoelectrode

The FE-SEM of WT-NTs is illustrated in Fig. 1. Figure 1a, b, c shows the top view of the sample formed by anodic oxidation in a DMSO-HF electrolyte containing 0.12 mM of sodium tungstate concentration. It can be seen that vertically ordered nanotubes with tube diameter in the range of 93 nm and wall thickness of 43 nm were formed on the surface of titanium foils. The surface of them was open. SEM images of WT-NTs from side view are illustrated in Figs. 1d, e, f. Cross-sectional view of the ordered nanotubes shows the formation of nanotubes with length in the range of 7.8 μm.

Figure 2a shows the XRD pattern of WT-NTs sample. It confirms the presence of anatase phase of TiO_2 in the sample. However, the diffraction pattern of WO_3 is not seen in the XRD of WT-NTs sample. This is likely due to a low composition of tungsten. Because tungsten oxide reflections were not observed in the diffraction patterns, an EDX spectrum of this sample was examined (Fig. 2b). In EDX spectrum of WT-NTs, peaks of Ti, W, and O were clearly observed and the contents of whom are present in Table 1. The presence of C species attributed to the absorption of carbon from the organic DMSO. This analysis confirms the presence of tungsten in the WT-NTs sample.

The optical properties such as reflectance spectra and optical band gap energy of WT-NTs were studied. Figure 3 shows the optical band gap energy of WT-NTs. The reflectance data, reported as $F(R)$ values, have been obtained by application of the Kubelka–Munk algorithm. The band gaps of the samples have been deduced from the Tauc plot. Figure 3 is the plot of $[F(R)h\upsilon]^{1/2}$ versus photon energy. The extrapolation of $[F(R)h\upsilon]^{1/2}$ to the abscissa at zero

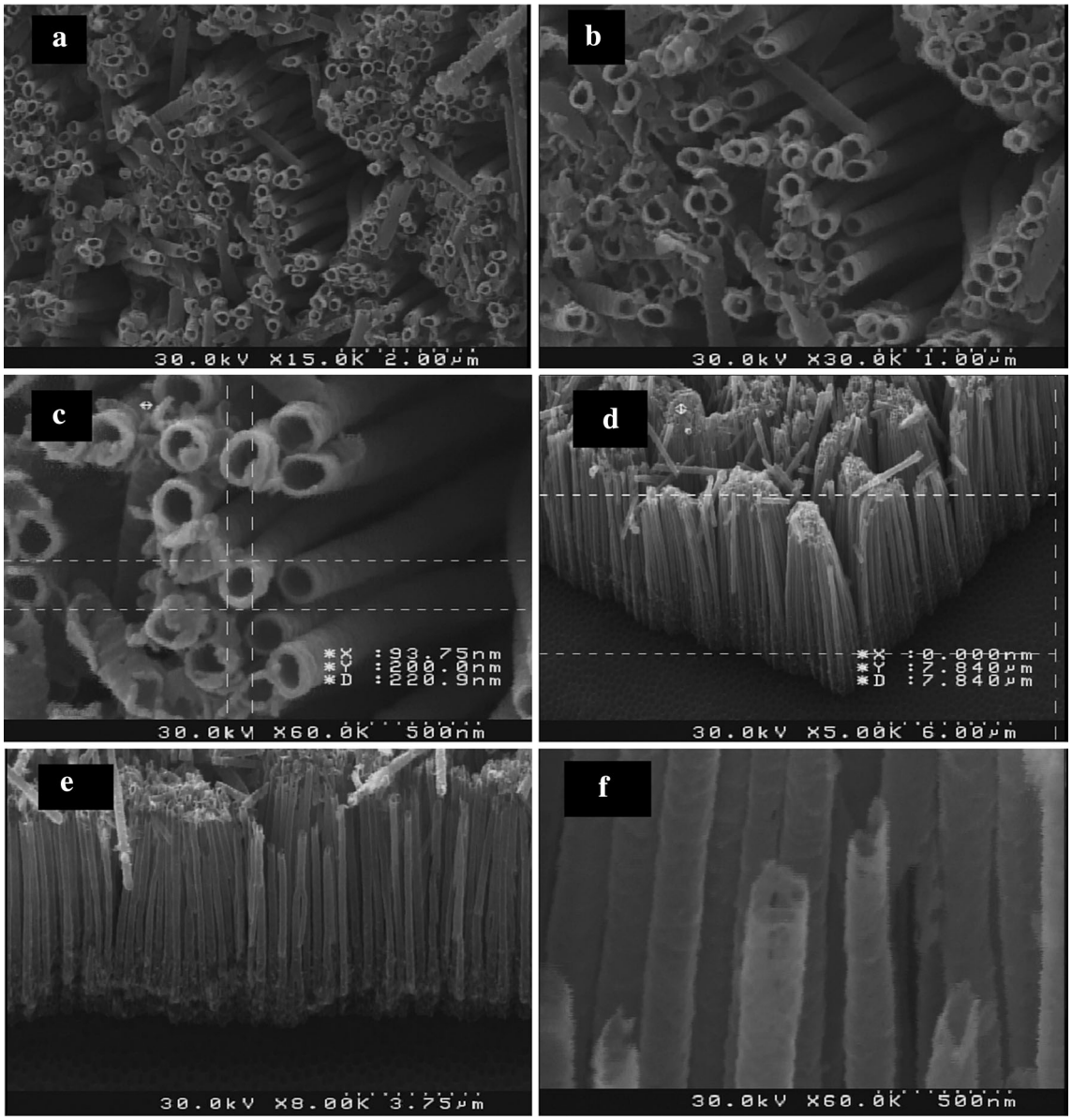

Fig. 1 **a–c** SEM top-view images of the WT-NTs sample and **d–f** cross-sectional images of this sample with different magnifications

F(*R*) provides the band gap energy as ~2.97 eV for WT-NTs and the band gap energy ~3.23 eV for unloaded TiO_2 samples [34]. The result indicates that WT-NTs sample has an optical absorption in the visible light region and a lower band gap energy due to the presence of WO_3 in TiO_2 and by coupling the TiO_2 nanotubes with WO_3, we were able to lower the band gap energy of unloaded TiO_2 from ~3.23 eV to the lower value. The red shift WT-NTs sample could be attributed to the formation of defect energy levels within the forbidden band of TiO_2 and also to the formation of new energy levels due to formation of W–O–Ti bonds in the solid solution of WO_3–TiO_2 during anodization process [40].

3.2 Degradation of 4-nitrophenol (4-NP)

3.2.1 *Photocatalytic activity of NTs and WT-NTs under visible light illumination*

Photocatalytic activity of two samples (NTs and WT-NTs) was followed through degradation of 4-NP as a function of irradiation time with visible light (Fig. 4a). First, 4-NP degradation experiments were conducted under visible light irradiation to evaluate direct photolysis without the addition of any catalyst. The concentration of 4-NP remained nearly constant after 120 min of irradiation. Thus, no obvious degradation of 4-NP was

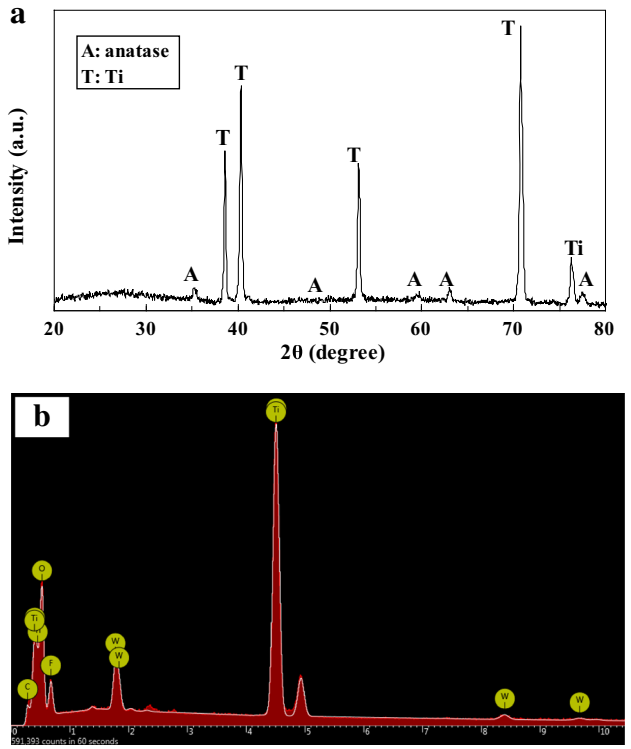

Fig. 2 **a** XRD pattern of WT-NTs sample annealed at 400 °C and **b** EDX spectra of this sample

Table 1 Average elemental compositions (at%) of pure TiO_2 and different TiO_2–WO_3 composites (samples A–D) obtained by taking five spots in EDX analysis

	Ti (at%)	*O* (at%)	*W* (at%)	*C* (at%)	*F* (at%)
Unloaded TiO_2	34.22	64.98	–	0.8	11.6
WT-NTs	24.8	49.9	8.6	0.3	16.4

observed in this time period. In addition, a dark control experiment was conducted, indicating that the adsorption of 4-NP onto the surface of the catalyst in the absence of visible light radiation was negligible. The photocatalysis results indicated that the photocatalytic process was very effective in the removal of 4-NP. Figure 4a shows the photocatalytic activity of two samples that were followed through degradation of 4-NP as a function of irradiation time with visible light. Under the irradiation of visible light, undoped NTs sample showed almost no photocatalytic activity, but WT-NTs sample showed photocatalytic activity. It can be said that due to the large band gap of NTs sample, it cannot absorb visible light, and so under these conditions, it does not have any photocatalytic properties.

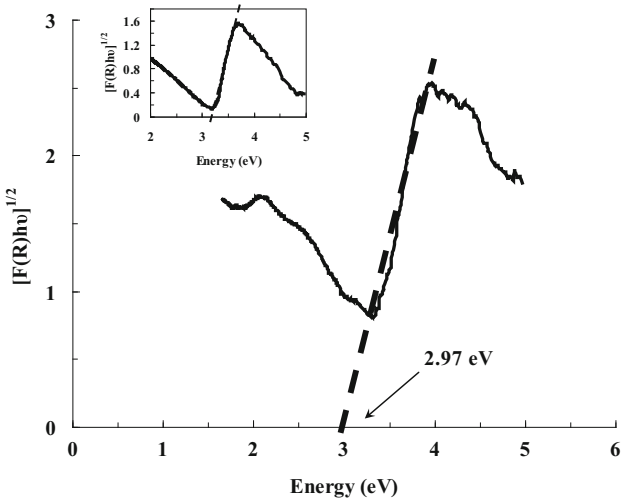

Fig. 3 $(Ah\upsilon)^{1/2}$ against hυ curve of the WT-NTs sample. (*Inset*) Plot of $(Ah\upsilon)^{1/2}$ versus $h\upsilon$ employed to calculate the band gap values of unloaded TiO_2

3.2.2 *Effect of photoelectrodes area on the degradation rates of 4-NP*

The evolution of photocatalytic degradation of 4-NP as a function of time in different reaction areas of WT-NTs photoelectrodes was done. The results showed that when the reaction areas were 1, 2, and 6 cm^2, the degradation percentages of 4-NP after 120-min illumination were 48, 71, and 96 %, respectively (Fig. 4b). The degradation percentage of 4-NP enhanced as the reaction area increases. The results indicated that the degradation percentage of 4-NP improved 48 % when the reaction area enlarged from 1 to 6 cm^2. It was well known that the amounts of photocatalyst increase with the increase in the reaction area and therefore the availability of active sites increases. When the photocatalyst increases, photogenerated electron–hole pairs increase too.

3.2.3 *Effect of initial pH*

The pH is an important factor that influences the removal of pollutants in aqueous solution. Sulfuric acid, sodium sulfate, and sodium hydroxide were used as electrolytes at this investigation, resulting in solutions with pH values of 2.21, 5.33, and 12.21, respectively. The conductivity of each solution was adjusted to be 1 mS/cm. The experimental conditions were the same with the former parts except the pH value (the reaction area was 2 cm^2). The degradation percentage of 4-NP by WT-NTs photoelectrodes in different pH are shown in Fig. 4c. It can be seen that the highest degradation ratio was achieved at the neutral conditions (in sodium sulfate electrolyte). The

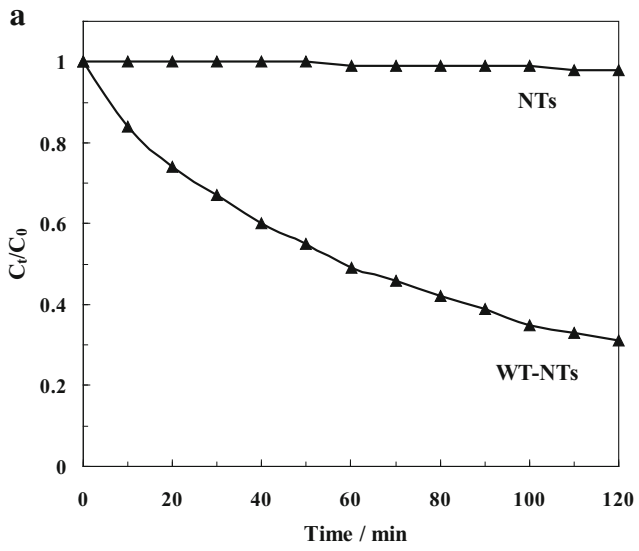
a
NTs
WT-NTs
C_t/C_0
Time / min

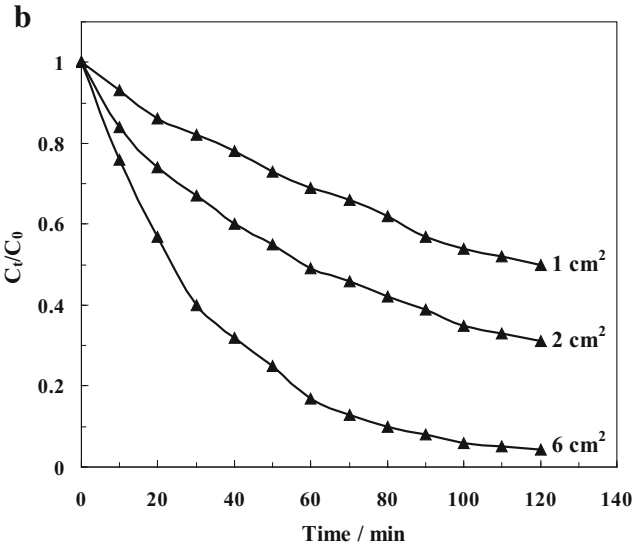
b
1 cm²
2 cm²
6 cm²
C_t/C_0
Time / min

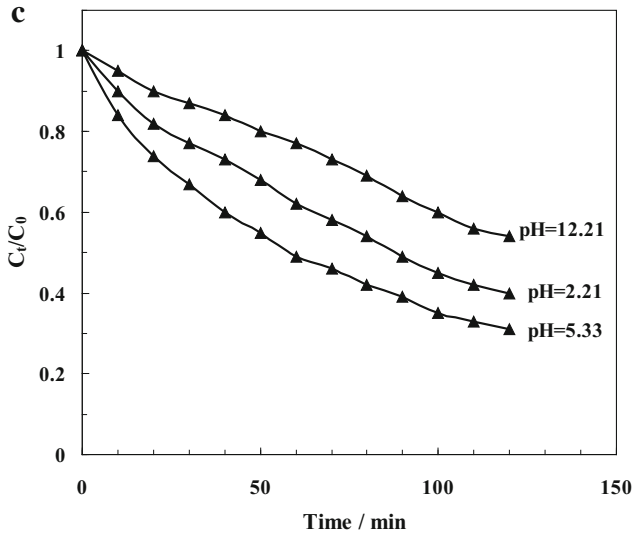
c
pH=12.21
pH=2.21
pH=5.33
C_t/C_0
Time / min

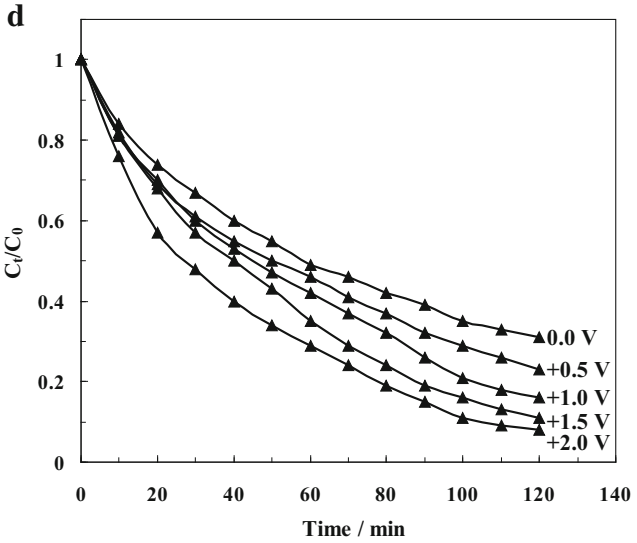
d
0.0 V
+0.5 V
+1.0 V
+1.5 V
+2.0 V
C_t/C_0
Time / min

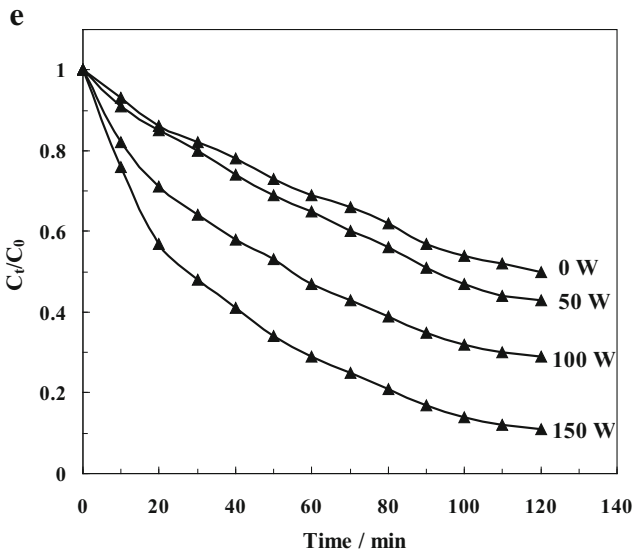
e
0 W
50 W
100 W
150 W
C_t/C_0
Time / min

◀**Fig. 4** **a**: Photocatalytic degradation of 4-NP over the different samples under visible light irradiation ($C_0 = 2$ mg/L, reaction area = 2 cm^2). **b**: Effect of photoelectrodes area on the degradation of 4-NP ($C_0 = 2$ mg/L). **c**: Effect of pH on the degradation rate of 4-NP ($C_0 = 2$ mg/L, reaction area = 2 cm^2). **d**: Effect of bias potentials on the degradations of 4-NP ($C_0 = 2$ mg/L, pH = 5.33, reaction area = 2 cm^2). **e**: Effect of the ultrasound power ($C_0 = 2$ mg/L, pH = 5.33, reaction area = 2 cm^2)

adsorption of organics depends on both the natures of photoelectrodes and the solutions, which would change with the pH of aqueous. For TiO_2 nanotubes photoelectrodes, the point of zero charge (PZC) was around 6.5 [41–43]. Under alkaline conditions, the potential of TiO_2 nanotubes was negative and 4-NP was also in an anion state. The coulombic repulsion between them would prevent the absorption of 4-NP on the photoelectrodes [41, 43]. Under acidic conditions, the surface of TiO_2 nanotubes was positive, which was an advantage to the adsorption of 4-NP and could promote the degradation of 4-NP. With the absorbance and then degradation of 4-NP, a lot H^+ would be produced [42]. Extra H^+ would positive-charge 4-NP and impacts its adsorption on the photoelectrodes; thus, its degradation rates decreased [41].

3.2.4 *Effect of external bias voltage on the photocatalytic reaction*

Anodic potential is one of important factors that affected the photocatalytic reaction. Positive potentials could drive photogenerated electrons on WT-NTs film to the counter electrode and then affect the degradation of 4-NP. Therefore, it is useful to have a study for selecting appropriate voltage in degradation of contaminants. In this section, the effect of applied bias voltage on the photoelectrocatalytic activity of WT-NTs photoelectrode is investigated, and the results show that with the increasing external potential, degradation rate of 4-NP increases gradually. With the positive potentials increasing, much more photogenerated electrons moved to the back contact or counter electrode. As a result, the recombination of photogenerated electron–hole pairs reduced, thus, more hydroxyl radicals ($^{\cdot}OH$) could be produced [44]. Accordingly, this process involved the decomposition of 4-NP. With the increase in bias potential, the separation efficiency of electron–hole pairs continuously enhanced and reached the maximum at the potential of +2.0 V (Fig. 4d). At the same time, as the potential increases, water could split slightly to produce active oxidizing free radicals or $^{\cdot}OH$ [42], which would also promote the decomposition of 4-NP. When the potential increased to +2.5 V, 4-NP degradation rate reduced. It is well known that at higher overpotential, hydroxyl radical would participate in the reaction to form oxygen; thus, its quantity to decompose 4-NP reduced [2, 41, 44, 45].

3.2.5 *Effect of the ultrasound power*

The degradation of 4-NP in sonophotocatalytic (SPC) processes with different ultrasonic power were done. The results show that after 120 min, 56, 71, and 89 % of 4-NP was removed when the ultrasonic power was 50, 100, and 150 W, respectively, which indicated that increasing ultrasonic power favored the degradation of 4-NP (Fig. 4e). The ultrasonic power of 150 W obtained the optimal sonophotocatalytic degradation efficiency of 4-NP.

3.2.6 *Comparison of different processes*

The sonophotoelectrocatalytic (SPEC), sonophotocatalytic (SPC), photoelectrocatalytic (PEC), and photocatalytic (PC) processes of 4-NP in aqueous solutions were performed on WT-NTs electrodes, as shown in Fig. 5. The applied potential in PEC and SPEC processes was +2.0 V, and ultrasound power of 150 W was used in SPC and SPEC processes. The photocatalytic process of 4-NP in 60 min was obviously much slower than sonophotocatalytic, photoelectrocatalytic, and sonophotoelectrocatalytic processes.

The sonophotocatalytic process of 4-NP was proven to enhance the photocatalytic efficiency because of the presence of ultrasound irradiation. In the presence of ultrasound, hydroxyl radical was generated from water division under the extreme pressure and temperature conditions

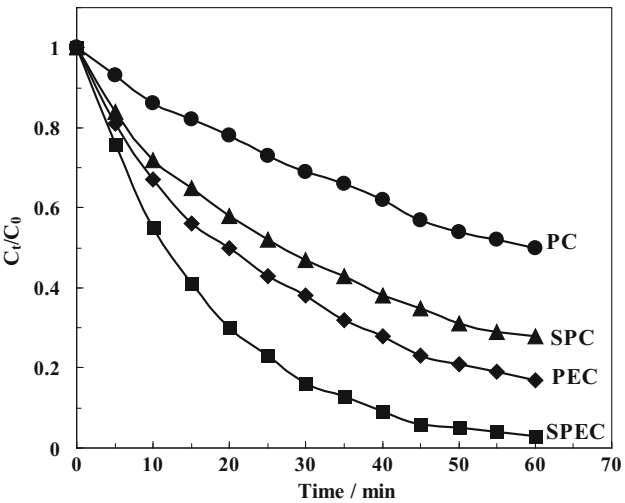

Fig. 5 Sonophotoelectrocatalytic (SPEC), photoelectrocatalytic (PEC), sonophotocatalytic (SPC), and photocatalytic (PC) processes of 4-NP degradation over WT-NTs electrode under visible light irradiation. $C_0 = 2$ mg/L, ultrasound power = 150 W, applied potential was +2.0 V

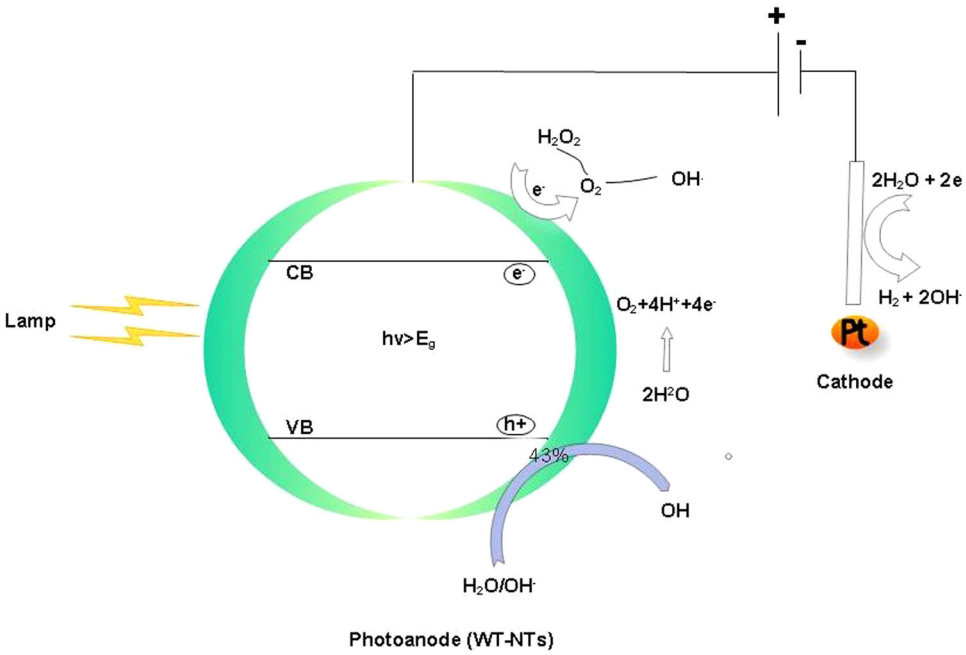

Fig. 6 Mechanism of photoelectrocatalytic process using WT-NTs photocatalyst and the reactions that occur at the surface

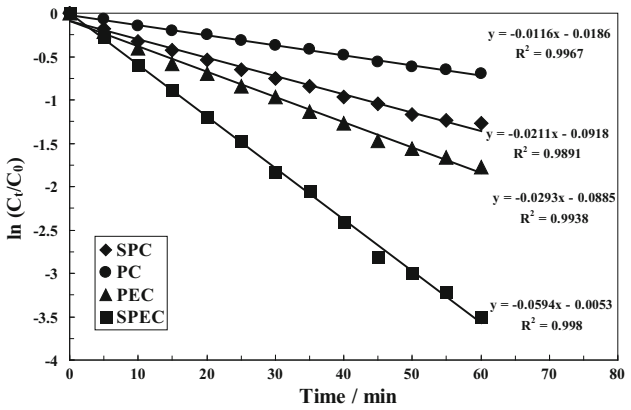

Fig. 7 Ln(C_t/C_0) versus irradiation time plot for PC, SPC, PEC, and SPEC processes of 4-NP degradation over WT-NTs electrode under visible light irradiation

created by the implosion of cavitation bubbles [8]. The hydroxyl radicals could oxidize organic matters in aqueous solutions and enhance the degradation efficiency of the 4-NP, which indicates the presence of a synergistic effect of photocatalysis and sonolysis. In general, the beneficial effect of coupling photocatalysis with sonolysis may be attributed to several reasons such as increased production of hydroxyl radicals in the reaction mixture, enhanced mass transfer of organics between the liquid phase and the catalyst surface, catalyst excitation by ultrasound-induced luminescence, and cleaning the surface of the catalyst in the presence of ultrasound waves.

The photoelectrocatalytic process of 4-NP with fast degradation efficiency was observed. The recombination of the photogenerated electron–hole pairs reduces the quantum efficiency and limits the application of photocatalysis in the field of wastewater treatment. In order to achieve good photocatalytic efficiency, recombination between electrons and holes must be avoided. It was possible that the recombination of photogenerated hole/electron pairs was suppressed by the external electric field, and thus the life of the holes and electrons got longer [8, 47]. There appears to be a synergistic effect between electrochemical processes and irradiation in the presence of semiconductor (WT-NTs). In fact, when a positive bias is applied to the WT-NTs photoanode, the generated electrons can be transferred into the external circuit. As a result, the photogenerated hole or OH• will be left at the surface of WT-NTs electrode. Therefore, the rate of photogenerated electron–hole recombination is limited, while a possibility exists to improve the efficiency oxidation at the semiconductor–electrolyte interface. In the photoelectrocatalytic process, the rate of conversion does not depend directly on the applied potential but depends on several factors such as the specific feature of the semiconductors, diffusion light, adsorption and desorption of the reactant and products, and the intensity of the electric field in the space charge region. According to these discussions, mechanism of the photoelectrocatalytic process and the main reaction that occurs at the surface of WT-NTs photoelectrodes is shown in Fig. 6.

Finally, the sonophotoelectrocatalytic process was checked and its degradation efficiency was the fastest among those processes studied. It was possibly because the ultrasound in photoelectrocatalytic process can enhance the degradation efficiency of photocatalytic process. To explain

this phenomenon, it can be said that there is a synergistic effect between ultrasound and photoelectrocatalytic.

The experimental data of Fig. 5 were found to fit approximately a pseudo-first-order kinetic model (Langmuir–Hinshelwood kinetic model) as follows:

$$\ln\left(\frac{C_t}{C_0}\right) = -kt \quad (10)$$

where C_t is the concentration of 4-NP at time t, C_0 is the equilibrium concentration after adsorption, and k is the rate constant. The values of the rate constant, k, and regression coefficient are inserted in Fig. 7. The reaction rate of SPEC process (0.0594 min^{-1}) was more than 5.1 times higher than that of PC process (0.0116 min^{-1}), 2.82 times higher than that of SPC process (0.0211 min^{-1}), and 2 times higher than that of PEC process (0.0293 min^{-1}). Therefore, there was an obvious synergistic effect among the electrochemical, sonolysis, and photocatalytic process.

The stability of a photocatalyst was also important to its practical application. We investigated the cyclic stability of WT-NTs electrode (in the SPEC process) by monitoring the catalytic activity during successive cycles of use (10-cycle experiment). The sample were rinsed carefully before starting a new test; after ten continuous runs for 4-NP degradation, the WT-NTs electrodes did not exhibit any significant loss of activity under this condition. The performance of the WT-NTs electrode showed a good reproducibility and retained the degradation rate of 95 % after 10 experiments for SPEC degradation of 4-NP in 60 min.

4 Conclusion

In the present work, WT-NTs photoelectrodes were fabricated by single-step anodization process, and morphology, crystal phase, chemical composition, and photocatalytic activity of the prepared samples were evaluated using various techniques. The effects of different parameters, such as reaction area, pH, bias potential, and ultrasound power, on photocatalytic activity of 4-nitrophenol (4-NP) in aqueous solutions in the presence of WT-NTs electrode were investigated. Also the photocatalytic degradation efficiency 4-NP in aqueous solutions showed a remarkable increase by means of simultaneous ultrasound and irradiation with electro-assisted way in the presence of this electrode. The rate constant of sonophotoelectrocatalytic was greater than that of both photoelectrocatalytic and sonophotocatalytic processes, indicating a synergistic effect among photo-, electro-, and sonoprocesses.

Acknowledgments The author would like to acknowledge the financial support of Iranian Nanotechnology Society and Isfahan University of Technology (IUT) Research Council.

References

1. T.E. Agustina, H.M. Ang, V.K. Vareek, J. Photochem. Photobiol. C **6**, 264 (2005)
2. R. Daghrir, P. Drogui, D. Robert, J. Photochem. Photobiol. A **238**, 41 (2012)
3. T.A. Egerton, J. Chem. Technol. Biotechnol. **86**, 1024 (2011)
4. G. Waldner, M. Pourmodjib, R. Bauer, M. Neumann-Spallart, Chemosphere **50**, 989 (2003)
5. R. Ojani, A. Khanmohammadi, J.B. Raoof, Mater. Sci. Semicond. Process. **31**, 651 (2015)
6. J. Madhavan, P.S.S. Kumar, S. Anandan, F. Grieser, M. Ashokkumar, Sep. Purif. Technol. **74**, 336 (2010)
7. F. Ahmedchekkat, M.S. Medjram, M. Chiha, A.M.A. Al-bsoul, Chem. Eng. J. **178**, 244 (2011)
8. Z. Zhang, Y. Yuan, L. Liang, Y. Fang, Y. Cheng, H. Ding, G. Shi, L. Jin, Ultrason. Sonochem. **15**, 370 (2008)
9. M.R. Hoffmann, S.T. Martin, W. Choi, D.W. Bahnemann, Chem. Rev. **95**, 69 (1995)
10. C.A. Martınez-Huitle, E. Brillas, Appl. Catal. B: Environ. **87**, 105 (2009)
11. Z.C. Wu, M.H. Zhou, Environ. Sci. Technol. **35**, 2698 (2001)
12. E. Kusvuran, A. Samil, O.M. Atanur, O. Erbatur, Appl. Catal. B: Environ. **58**, 211 (2005)
13. H.G. Oliveira, D.C. Nery, C. Longo, Appl. Catal. B: Environ. **93**, 205 (2010)
14. A. Babuponnusami, K. Muthukumar, J. Environ. Chem. Eng. **2**, 557 (2014)
15. N.N. Mahamuni, Y.G. Adewuyi, Ultrason. Sonochem. **17**, 990 (2010)
16. K.P. Wang, J.S. Guo, M. Yang, H. Junji, R.S. Deng, J. Hazard. Mater. **162**, 1243 (2009)
17. Y.Z. Ren, Z.L. Wu, M. Franke, P. Braeutigam, B. Ondruschka, D.J. Comeskey, P.M. King, Ultrason. Sonochem. **20**, 715 (2013)
18. R. Kidak, N.H. Ince, Ultrason. Sonochem. **13**, 195 (2006)
19. Z.L. Wu, B. Ondruschka, G. Cravotto, Environ. Sci. Technol. **42**, 8083 (2008)
20. J.G. Lin, C.N. Chang, J.R. Wu, Y.S. Ma, Water Sci. Technol. **34**, 41 (1996)
21. B. Neppolian, H. Jung, H. Choi, J.H. Lee, J.W. Kang, Water Res. **36**, 4699 (2002)
22. P. Braeutigam, M. Franke, R.J. Schneider, A. Lehmann, A. Stolle, B. Ondruschka, Water Res. **46**, 2469 (2012)
23. R. Chand, N.H. Ince, P.R. Gogate, D.H. Bremner, Sep. Purif. Technol. **67**, 103 (2009)
24. G.H. Zhao, J.X. Gao, S.H. Shen, M.C. Liu, D.M. Li, M.F. Wu, Y.Z. Lei, J. Hazard. Mater. **172**, 1076 (2009)
25. I. Paramasivam, J.M. Macak, P. Schmuki, Electrochem. Commun. **10**, 71 (2008)
26. K.P. Xie, L. Sun, C.L. Wang, Y.K. Lai, M.Y. Wang, H.B. Chen, C.J. Lin, Electrochim. Acta **55**, 7211 (2010)
27. X.L. He, Y.Y. Cai, H.M. Zhang, C.H. Liang, J. Mater. Chem. **21**, 475 (2011)
28. G.K. Mor, O.K. Varghese, R.H.T. Wilke, S. Sharma, K. Shankar, T.J. Latempa, K.S. Choi, C.A. Grimes, Nano Lett. **8**, 1906 (2008)
29. G.K. Mor, H.E. Prakasam, O.K. Varghese, K. Shanker, C.A. Grimes, Nano Lett. **7**, 2356 (2007)
30. M.G. Hosseini, M.M. Momeni, M. Faraji, Electroanalysis **23**, 1654 (2011)
31. Z. Jiang, F. Yang, N.J. Luo, B.T.T. Chu, D. Sun, H.H. Shi, T.C. Xiao, P. Edwards, Chem. Commun. **47**, 6372 (2008)
32. S.Y. Kuang, L.X. Yang, S.L. Luo, Q.Y. Cai, Appl. Surf. Sci. **255**, 7385 (2009)
33. M.M. Momeni, Y. Ghayeb, M. Davarzadeh, J. Electroanal. Chem. **739**, 149 (2015)

34. A. Kongkanand, K. Tvrdy, K. Takechi, M. Kuno, P.V. Kamat, J. Am. Chem. Soc. **130**, 4007 (2008)
35. M.G. Hosseini, M.M. Momeni, Appl. Catal. A **427**, 35 (2012)
36. A. Lewera, L. Timperman, A. Roguska, N. Alonso-Vante, J. Phys. Chem. C **115**, 20153 (2011)
37. C.W. Lai, S. Sreekantan, E.P. San, W. Krengvirat, Electrochim. Acta **77**, 128 (2012)
38. C. Das, I. Paramasivam, N. Liu, P. Schmuki, Electrochim. Acta **56**, 10557 (2011)
39. K.I. Liu, Y.C. Hsueh, C.Y. Su, T.P. Perng, Int. J. Hydrog. Energy **38**, 7750 (2013)
40. Y. Xin, M. Gao, Y. Wanga, D. Ma, Chem. Eng. J. **242**, 162 (2014)
41. J. Gong, C. Yang, W. Pu, J. Zhang, Chem. Eng. J **167**, 190 (2011)
42. L. Pinhedo, R. Pelegrini, R. Bertazzoli, A.J. Motheo, Appl. Catal. B: Environ. **57**, 75 (2005)
43. J. Grzechulska, A.W. Morawski, Appl. Catal. B: Environ. **36**, 45 (2004)
44. M.V.B. Zanoni, J.J. Sene, M.A. Anderson, J. Photochem. Photobiol. A **157**, 55 (2003)
45. H. Hidaka, J.C. Zhao, E. Pelizzetti, N. Serpone, J. Phys. Chem. **96**, 2226 (1992)